**Mineral reactivity:
from biomineralization and Earth's climate evolution
to CO₂ capture and monument conservation**

Influence of gel-strength and magnesium doping on the organization of calcite/hydrogel mesocrystal composites

Fitriana NINDIYASARI[1], Lurdes FERNÁNDEZ-DÍAZ[2,3], Xiaofei YIN[4], Martina GREINER[4],
Erika GRIESSHABER[4,*], Meaza TSIGE[5], Andreas ZIEGLER[6] and Wolfgang W. SCHMAHL[4]

[1]NRG, Westerduinweg 3, 1755 Le Petten, The Netherlands
*Corresponding author, e-mail: e.griesshaber@lrz.uni-muenchen.de
[2]Departamento de Mineralogía y Petrología, Universidad Complutense de Madrid, 28040 Madrid, Spain
[3]Instituto de Geociencias (UCM, CSIC), C/José Antonio Novais 2, 28040 Madrid, Spain
[4]Department für Geo- und Umweltwissenschaften Ludwig-Maximilians-Universität, 80333 Munich, Germany
[5]Departamento de Geodinámica, Estratigrafía y Paleontología, Universidad Complutense de Madrid,
28040 Madrid, Spain
[6]Central Facility for Electron Microscopy, University of Ulm, 89069 Ulm, Germany

Abstract: Calcite growing in biomimetic hydrogel environments incorporates the gel during its growth. The amount of occluded gel within the composite is mainly determined by the interaction between gel strength and crystallization pressure, with the latter being directly related to supersaturation and growth rate. In previous work we established a direct correlation between increased amounts of occluded gel with misorientations in the growing calcite crystals or aggregates. The presence of Mg^{2+} in the growth environment adds complexity to the internal structuring of the mineral. In this contribution we examine the effects of Mg^{2+} on the mechanical parameters of gelatin hydrogel and silica hydrogel by mechanical shear stress tests, we determine characteristics of the gel fabric occluded in the calcite using selective etching techniques and high-resolution field emission scanning electron microscope (FE-SEM) imaging, and we use electron backscatter diffraction (EBSD) to study co-orientation or misorientation in the calcite crystals or aggregates. We show that two independent mechanisms are responsible for the complex impact of Mg^{2+} in the growth medium on the calcite/gel composites. First, addition of 0.1 M Mg^{2+} reduces the yield-strength of the gels by about 50%. While gelatin gel shows continuous strain hardening in a similar way for Mg-bearing and Mg-free systems, the silica-gel weakens after reaching an ultimate shear strength, where the strain associated with the maximum in strength shifts by 350% to higher values. The decreased gel strength in the Mg-bearing systems leads to decreased amounts of occluded gel. Second, incorporation of Mg^{2+} in the growing calcite (i) increases its solubility and thus decreases crystallization pressure, and (ii) introduces small angle grain boundaries due to misfit strains which lead to "split growth", *i.e.* misoriented subunits of the calcite or – ultimately – spherulitic growth. Our study further clearly shows that Mg not only influences the organization of the mineral component within the aggregate but also the fabric of the occluded gel matrix. The fabrics of the occluded gel change from compact gel membranes to finely dispersed networks with increasing Mg and, correspondingly, decreased crystallization pressure *via* increasing solubility as more Mg incorporates into calcite structure. This circumstance initiates the large variety of calcite crystal co- and misorientation patterns and hierarchical assemblies that we find in the investigated composites.

Key-words: biomimetic crystallization; calcite-gel composites; shear strength; EBSD.

1. Introduction

The understanding of factors that control biomineralization has greatly advanced in the last decades, due to the in-depth characterization of the organic and inorganic components that constitute numerous biological hard tissues at different scale levels (Weiner & Traub, 1980; Fritz & Morse, 1998; Blank *et al.*, 2003; Marin & Luquet, 2004; Robach *et al.*, 2005; Addadi *et al.*, 2006; Nudelman *et al.*, 2006; Fratzl & Weinkamer, 2007; Griesshaber *et al.*, 2007; Marin *et al.*, 2008; Sethmann & Worheide, 2008; Alvares *et al.*, 2009; Robach *et al.*, 2009; Checa *et al.*, 2011; Goetz *et al.*, 2011; Gries *et al.*, 2011; Seidl *et al.*, 2011; Li *et al.*, 2011b; Sunaband & Bhushan, 2012; Bar-On & Wagner, 2013; Dunlop & Fratzl, 2013; Griesshaber *et al.*, 2013; Goetz *et al.*, 2014; Huber *et al.*, 2014). This understanding has been further promoted by the results of biomimetic crystallization experiments conducted under well-defined conditions (García-Ruiz *et al.*, 1995; Grassmann *et al.*, 2002; Han *et al.*, 2005; Cheng & Gower, 2006; Wang *et al.*, 2006; Pokroy & Aizenberg, 2007; Huang *et al.*, 2008; Otalora *et al.*, 2009; Nindiyasari *et al.*, 2014a, b, 2015) as well as

recent experimental and theoretical developments that have identified the role of amorphous precursors in the formation of biominerals (Cölfen & Antonietti, 2008; Gower, 2008; Meldrum & Cölfen, 2008; Cölfen, 2010; Dey *et al.*, 2010; Gebauer & Cölfen, 2011; Weiner & Addadi, 2011; Wolf *et al.*, 2011; Cartwright *et al.*, 2012). Further advances can be expected to result from the application of methodologies typically used in the study of biological hard tissues for the characterization of organic-inorganic composites formed in biomimetic systems under controlled conditions (Sethmann *et al.*, 2007; Li *et al.*, 2009; Kim *et al.*, 2014; Nindiyasari *et al.*, 2014a, b, 2015).

Most biomineralization processes occur in chemically complex water-rich gelatinous environments which contain different proportions of polysaccharides, proteins and glycoproteins (Lowenstam & Weiner, 1989; Mann, 2001). This common characteristic that is shared by both, biomineralization environments and artificial hydrogels, render the latter as excellent model systems for conducting biomimetic experiments (García-Ruiz, 1991; Grassmann *et al.*, 2002; Sugawara *et al.*, 2003; Simon *et al.*, 2004; Dorvee *et al.*, 2012). Several studies have proven that hydrogels are versatile systems that can be fine-tuned in order to resemble more closely the characteristics of biological mineralization environments (Fernández-Díaz *et al.*, 1996; Kosanovic *et al.*, 2011; Asenath-Smith *et al.*, 2012; Sancho-Tomás *et al.*, 2013, 2014a, b). A wide variety of hydrogels are used for biomimetic crystallization experiments, among which polyacrylamide, silica, agarose and gelatin gels are currently studied most (Henisch, 1988; Kniep & Simon, 2007; Helbig, 2008). Specific characteristics of the different hydrogels differ significantly depending on aspects such as the reversibility or irreversibility of the gelation process (physical or chemical hydrogels), the interactions that hold their matrices together, their porosity, and the absence or presence of functional groups on their pore walls (Asenath-Smith *et al.*, 2012).

One of the most common carbonate components of biological hard tissues is calcite. Depending on phyla, calcite can incorporate magnesium in concentrations which are widely variable (Lowenstam & Weiner, 1989; Aizenberg *et al.*, 1995; Mann, 2001; Bentov & Erez, 2006; Politi *et al.*, 2006). In previous work we used different hydrogels in Mg-free and Mg-bearing biomimetic environments to grow calcite-gel composites (Nindiyasari *et al.*, 2014a, b) and studied characteristics of composite formation and composite aggregate growth. Electron backscatter diffraction (EBSD) measurements performed on these composites evidenced internal structuring, that is significantly more complex in composites formed in organic hydrogels like gelatin, agar or agarose than in those grown in silica hydrogel (Nindiyasari *et al.*, 2015; Greiner *et al.*, 2018). We attributed characteristics of this structuring as being partially related to the different distribution patterns of the occluded hydrogel network within the mineral component. We interpreted this feature to be the consequence of the different mechanical response of the hydrogel matrix to crystallization pressure (Nindiyasari *et al.*, 2015; Greiner *et al.*, 2018). For composites grown in gelatin hydrogels we confirmed a direct correlation between gel solid content and the amount of

incorporated gel matrix into the calcite as well as the complexity of the calcite-gelatin gel structuring (Nindiyasari *et al.*, 2014a). This correlation strongly relates to the change in mechanical properties of the gel (gel strength) as it becomes denser. Furthermore, by adding a 0.1 M $MgCl_2$ containing solution to gelatin, agarose and silica hydrogel, we can state that the presence of Mg in the growth medium influences the structuring of calcite-hydrogel composites by contributing to the development of low and high angle boundaries between crystal subunits and promoting split growth phenomena (Nindiyasari *et al.*, 2014b, 2015).

In the work presented here we focus on two different hydrogels: (i) gelatin, a chemical gel, and (ii) silica, a physical gel. We deepen our understanding of the influence of Mg in the organization of calcite-gel composites by studying aggregates formed in the presence of different Mg concentrations in the growth medium: without Mg, with a low (0.01 M) and a high (0.1 M) Mg concentration. By comparing the characteristics of the obtained composite aggregates, we aim to distinguish between those effects that can be related to the incorporation of Mg into the calcite structure from effects where the presence of Mg induces changes in the mechanical properties of the gels, thereby affecting the pattern of gel occlusion during calcite growth. Our goal in this study is to investigate which factor has a greater influence on the formation of different calcite micro- and mesostructures: gel occlusion or Mg incorporation into the calcite, and to determine whether an interaction between these two factors does exist.

2. Experimental procedure

2.1. Crystal growth

Crystallization experiments were conducted using the double diffusion variant of the hydrogel method (Henisch, 1988). The hydrogel occupies the horizontal branch of a U-tube, while reagents fill its vertical branches (Sancho-Tomás *et al.*, 2014a). Crystallization occurs within the hydrogel column by chemical reaction following counter diffusion of the reagents (0.5 M $CaCl_2$ and 0.5 M Na_2CO_3; Sigma Aldrich). In our experimental setup the hydrogel column was 120 mm long and 9 mm in diameter and the volume of each reagent aqueous solution was 5 mL. We conducted experiments using two types of hydrogels, silica and gelatin, and considered absence of Mg, and low (0.01 M) as well as high (0.1 M) concentrations of Mg in the growth medium. Silica hydrogel was prepared by acidifying a sodium silicate solution (Merck, sp. gr.: 1.509 g cm^{-3}; pH = 11.2) to pH = 5.5 by slow addition of HCl (1N) under constant stirring. Magnesium-bearing silica hydrogels were prepared by adding adequate volumes of a $MgCl_2$ solution to the silica sol prior to gelation. Gelation took place at 15 °C. Mg-free and Mg-bearing gelatin hydrogels were prepared by dissolving porcine gelatin (Sigma Aldrich; Type A, Bioreagent) in water and in 0.01 M and 0.1 M $MgCl_2$ aqueous solutions, previously heated at 60 °C. The concentration of gelatin in the hydrogel was 10 wt %. Gelation took place at 4 °C for one hour. In all the cases,

hydrogels were left to set for 24 h at 15 °C after gelation before pouring the reagent solutions in the deposits. All experiments were conducted at 15 °C and run triplicate. All solutions were prepared using high purity deionized (Milli-Q) water.

The extraction of calcite-gel composites from silica hydrogel was carried out by dissolving the slice of hydrogel where these composites are located in a 1 M NaOH solution for 20 min. Afterwards, the composites were thoroughly rinsed with Milli-Q water, placed in an ultrasonic bath for 10 min to remove rests of silica hydrogel adhered to the composites' surfaces, rinsed again and finally left to dry at room temperature. In the case of gelatin hydrogel, the gel slice containing composites was dissolved in hot water (60 °C). Composites were collected after filtration through a 1-μm pore size membrane, thoroughly rinsed with hot Milli-Q water and dried at room temperature.

2.2. Calcite–gel composites morphological characterization

Calcite–gel composites formed in Mg-free and Mg-bearing silica and gelatin hydrogel were selected under a binocular stereomicroscope and hand-picked using a fine painting brush. The crystals were then mounted on holders, coated with gold and/or carbon. Scanning electron microscopy (SEM) images of these composites were obtained using JEOL JSM6400 (40 kV) and JEOL JSM335F (30 kV) microscopes equipped with energy dispersive spectrometers (LINK Ex1; Oxford Instruments 80 mm^2 X-Max SDD). In the case of calcite-silica hydrogel composites, a conservative treatment meant to avoid any alteration of their surfaces was followed during their separation from the hydrogel. As a result, small amounts of silica hydrogel remained on the surface of some of the aggregates, which negatively affected the quality of some of the SEM images.

2.3. Preparation for SEM imaging of the etched crystal/hydrogel composites

The preparation was started by gluing the crystal on the aluminium cylinder holder. The samples were first cut using an Ultracut ultramicrotome (Leica) using glass knifes to obtain plane surfaces within the material, as close as possible to an equatorial plane of the crystal aggregate. In the case of samples grown in silica hydrogel, these surfaces were cut either approximately parallel to (104), when their habit approached a rhombohedron, or through their largest axis, when aggregates showed dumbbell-like morphologies. These surfaces were then polished with a diamond knife (Diatome) by stepwise removal of material in a series of sections with successively decreasing thicknesses (90 nm, 70 nm, 40 nm, 20 nm, 10 nm and 5 nm, each step was repeated 15 times) (Fabritius et al., 2005; Nindiyasari et al., 2014a, b, 2015). The polished crystals were etched using 0.1 M HEPES (pH = 6.5) containing 2.5% glutaraldehyde as a fixation solution. The etching time was 90 s. The etched samples were then dehydrated in 100% isopropanol for 10 s three times and critical point dried in a BAL-TEC CPD 030 (Liechtenstein). The etched samples were imaged using a Hitachi S5200 field emission scanning electron Microscope (FE-SEM) at 4 kV after drying and rotary coating with 3 nm platinum.

2.4. Preparation for electron backscatter diffraction (EBSD) of the decalcified crystal/hydrogel composites

EBSD measurements required a highly even surface. The composites were embedded into EPON resin and were polished using diamond suspension down to a grain size of 1 μm. The final polishing was performed using silica etch-polishing with colloidal silica (particle size ~ 0.06 μm). The polished samples were coated with 4 nm of carbon. The EBSD measurement was run at 20 kV on a FEG-SEM (JEOL JSM 6400) equipped with an Oxford Instruments NordlysNano EBSD detector.

2.5. Hydrogel shear stress characterization

Circular samples, 50 cm in diameter and 2.5 cm height, of Mg-free and Mg-bearing (0.01 M and 0.1 M) gelatin and silica hydrogels were prepared by pouring the corresponding sol in a metallic mold. After gelation took place the samples where left to set for 18 h. They were then placed in a shear box, within a deformation ring. This box comprises two parts: an upper one, which remains fixed, and a lower one, which can be horizontally displaced. Shear strength measurements were conducted on the gel samples at 25 °C and under dry conditions using the standard Direct Shear Test configuration (ASTM D 3080, 2011). This configuration involves applying a direct shear stress (τ), which results in the sample sliding along a defined horizontal failure plane at a constant rate (0.05 mm min^{-1}). A constant vertical load was applied (σ_n = 33 kPa) in the case of gelatin gels. Measurements on silica gels were performed without vertical load to avoid both, vertical deformation and high water loss. The resulting horizontal displacement was continuously recorded at a constant rate during the test. The experiment was stopped after the samples had reached 20% horizontal deformation. The shear and normal stress data were calculated considering the decreasing area of contact between the upper and lower surfaces of the sample as the displacement progressed. The maximum shear stress required to cause slip (shear strength τ_f), as well as the shear-strain evolution of the six gel samples were estimated from the variation of the shear stress as a function of the horizontal movement.

3. Results

3.1. Morphologies and composition of gel/calcite composites grown in Mg-free and Mg-bearing silica and gelatin hydrogels

Morphological features of calcite-gel composites strongly vary with the type of hydrogel that is used, but are also affected by the presence of Mg in the growth medium
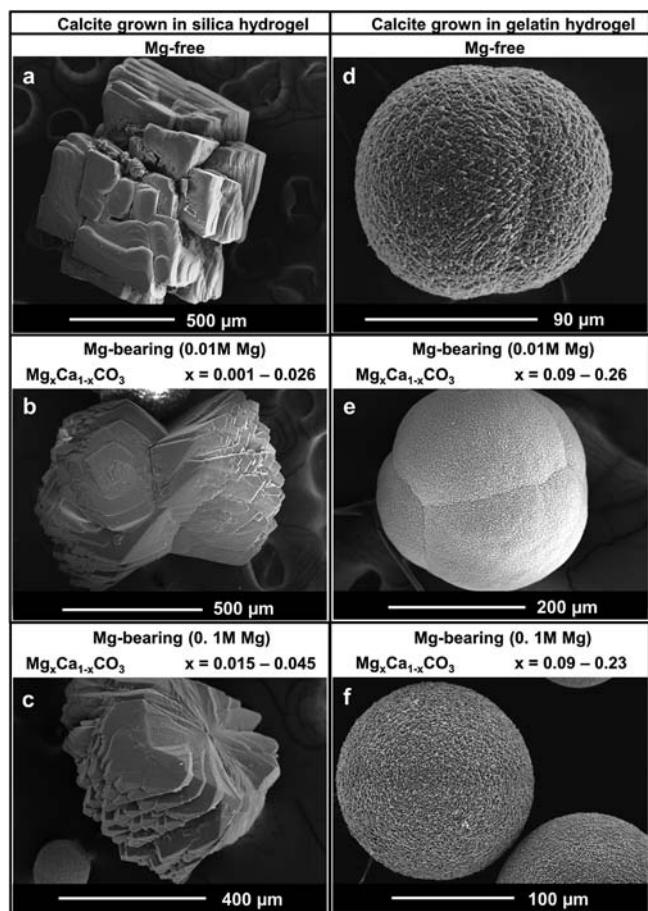
Fig. 1. FE-SEM images of calcite/gel composites grown in silica (a–c) and gelatin (d–f) hydrogels without (a, d) and with Mg (b, c, e, f). (a) Hopper crystal bounded by strongly terraced (104) surfaces grown in Mg-free silica hydrogel. (b) Dumbbell-like composite grown in 0.01 M $MgCl_2$-bearing silica hydrogel. Note the equatorial cleft and the radial arrangement of units. (c) Dumbbell-like composite grown in 0.1 M $MgCl_2$-bearing silica hydrogel. Note that the composite is broken through the equatorial cleft and the image corresponds to a half of the dumbbell. EDX analyses on the surface of the composites in (b) and (c) yield Mg contents around 1 and 3 mol% $MgCO_3$, respectively. (d) Pseudospherical calcite-gel composite formed in Mg-free gelatin hydrogel. (e) Curved-surfaced calcite-gel composite formed in 0.01 M Mg-bearing gelatin hydrogel. (f) Sphere-like calcite-gel composite formed in a 0.1 M $MgCl_2$-bearing gelatin hydrogel. EDX analyses on the surface of composites shown in (e) and (f) yield Mg contents around 15 and 17 mol% $MgCO_3$, respectively.

(Figs. 1 and 2). Composites grown in Mg-free silica hydrogel appear as hopper crystals with strongly terraced (104) surfaces and edges that are alternatingly straight and curved, reproducing the calcite $\bar{3}$ fold axis (Fig. 1a). When $MgCl_2$ is added to the silica gel, calcite/gel composites show a dumbbell-like morphology characterized by a marked equatorial cleft. This morphology results from the radial arrangement of flat-surfaced units bounded by highly stepped rhombohedron faces (Fig. 1b, c). Differences in the concentration of $MgCl_2$ in the hydrogel are reflected by slight microstructural changes of the composites, with those formed in the presence of higher $MgCl_2$ concentration consisting of a higher number of mutually misoriented units (Fig. 1b, c). EDX analyses taken on the surfaces of these composites yield Mg contents that are in the range 0.1–2.6 mol% $MgCO_3$ in those grown in 0.01 M Mg-bearing silica hydrogel and 1.5–4.5 mol% $MgCO_3$ in those formed in 0.1 M Mg-bearing silica hydrogel.

Calcite/gel composites grown in Mg-free gelatin hydrogel show dumbbell-like to spherical morphologies (Fig. 1d). Composites formed in $MgCl_2$-bearing gelatin hydrogels have a variety of morphologies which range from radial spherulites to sphere-like aggregates (Fig. 1b, e) and from dumbbell- to sphere-like aggregates (Fig. 1c, f) in gelatin hydrogel bearing 0.01 M and 0.1 M $MgCl_2$, respectively. In both cases (0.01 M and 0.1 M $MgCl_2$ in the gelatin hydrogel) sphere-like aggregates are the most common. Figure 1e and f shows this type of composites that are formed in gelatin bearing 0.01 M and 0.1 M $MgCl_2$, respectively. EDX analyses collected on the surfaces of sphere-like calcite/gelatin composites yield Mg contents that varied between 10 mol% and well above 20 mol% $MgCO_3$ in both composites grown in gelatin with 0.01 M and 0.1 M $MgCl_2$.

3.2. Hydrogel fabric and the micro- and mesoscale structures of the composite aggregates

Figure 3 shows the mesoscale composite nature of the investigated gel/mineral aggregates obtained without (Fig. 3a, d) and with Mg (Fig. 3b–d, f) in the growth medium. In the case of silica gel (Fig. 3a–c) we observe that the size of the mineral units in the composite decreases with the addition of magnesium. Thus, high concentrations of Mg in the growth medium appear to have the effect that the silica network is more dispersed in the silica gel/calcite aggregate.

In gelatin gel/calcite aggregates (Fig. 3d–f) we observe the occlusion of gel membranes and fibres. In Mg-free growth environments (Fig. 3d), thick gelatin gel membranes are occluded and separate individual and large calcite sub-units of the aggregate from each other. A small amount of Mg evokes the formation of irregular membranes within the aggregates (Fig. 3e). These are thinner in comparison to those present in aggregates grown without Mg in the growth medium and form irregularly shaped and sized compartments that are filled with calcite. A fine network of gelatin gel fibres fills the space between calcite crystallites. For high $MgCl_2$ concentration (0.1 M) in the growth medium gelatin gel membranes are not observed in the gel/calcite aggregate. The fabric of the gel constitutes a fibre network well visible between blocky calcite units.

Figure 4 highlights calcite co- and misorientation derived from EBSD measurements. Figure 4a–c shows orientation results obtained for aggregates grown in silica gel, while Fig. 4d–f shows calcite orientation in aggregates that were obtained in gelatin gel. Calcite orientation is presented colour-coded with EBSD maps and corresponding pole figures. In the Mg-free case we observe a good, single-crystal-like co-orientation of the calcite in the mesocrystal composite over distances of more than 100 μm (Fig. 4a, d).
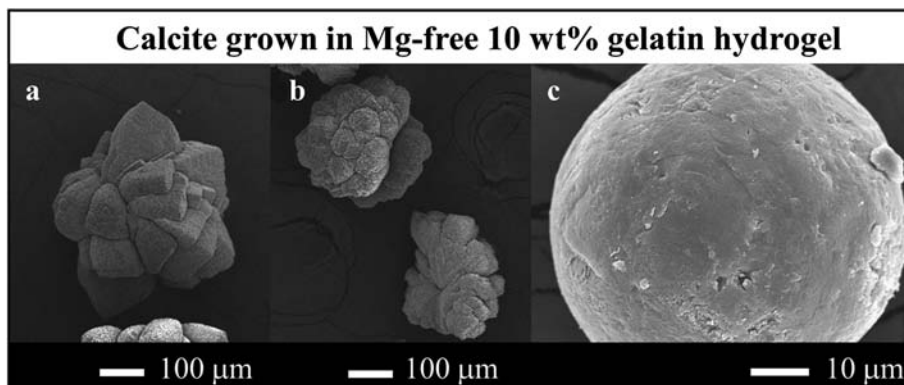
Fig. 2. The wide variety of aggregate morphologies obtained in growth experiments carried out with 10 wt% gelatin in an Mg-free environment.

With the addition of $MgCl_2$ and the increase of its concentration in the silica gel, crystal co-orientation decreases and a radial aggregate consisting of a few subunits (Fig. 4c) is formed. In the case of aggregates grown in gelatin gel, as Mg concentration in the growth medium increases we observe the change from radial aggregates that comprise few subunits (Fig. 4b, e) to spherulites (Fig. 4f) (this work and see also Nindiyasari *et al.*, 2015). As Fig. 4b, e shows, even the presence of low Mg contents in the growth medium highly influences the mesoscale structure of the aggregate, an effect that is most pronounced when the aggregate grows in gelatin gel.

Figure 5 graphically summarises and highlights the different influence of both, the type of hydrogel and the concentration of Mg in the growth medium in defining the characteristics of calcite assembly (Fig. 5a–f) and the composite aggregate microstructure (Fig. 5g).

Texture sharpness, the strength of calcite co-orientation, is expressed with MUD values. The MUD value is defined as the multiple of uniform (random) orientation (Kocks *et al.*, 2000). A calcite single crystal precipitated from solution, devoid of any gel, has a MUD value of 725 (Kim *et al.*, 2014; Nindiyasari *et al.*, 2014b, Greiner *et al.*, 2018). The mesocrystalline calcite grown in silica and gelatin gels shows a mainly single-crystal-like co-orientation despite the gel occlusion. Furthermore, the occlusion of both gels seems to have an almost negligible effect, especially that of silica gel, on calcite misorientation (Fig. 5a: MUD of silica gel grown aggregate: 690; MUD of gelatin gel grown aggregate: 590). In addition, the different effects that the gels exert on the co-orientation or misorientation of calcite crystals in the aggregate is also well observable. As the lower MUD value of the aggregate grown in gelatin gel compared to that grown in silica gel shows, Mg-free gelatin gel does exert a slight influence on calcite crystal assembly and promotes a slight misorientation between calcite crystallites. Silica gel, on the other hand, has almost no detrimental effect on co-orientation (MUD: 690 *vs*. 725 for calcite precipitated in solution). The concomitant decrease of MUD values coupled to an increase in Mg content in the case of silica gel is well demonstrated in Fig. 5b, c and g. For gelatin gel we see a slightly different behaviour.

As Fig. 5e, f and especially Fig. 5g highlight, even a small addition of $MgCl_2$ to gelatin gel has a drastic effect on calcite organization and causes significant misorientation between the crystallites in the aggregate.

3.3. Mechanical behaviour of silica and gelatin gels

The macroscopic mechanical response of silica and gelatin hydrogels, both Mg-free and Mg-bearing was studied by conducting direct shear stress tests. The shear stress-shear strain curves of gelatin gels, both Mg-free and Mg-bearing (0.01 M and 0.1 M) are depicted in Fig. 6a. The three curves are characterised by an initial elastic stage, with a high shear modulus, which is followed by a strain hardening behaviour with progressive deformation. This behaviour is similar for the three studied gelatin samples. The characteristics of the three shear strength-strain curves are consistent with gelatin gels showing an elasto-plastic mechanical behaviour, regardless the concentration of $MgCl_2$ added to the gel. Differences between the three gels refer to the strain stage for yielding point (point where the elastic behaviour is lost), which is higher in the Mg-free gelatin gel and becomes smaller as the Mg content increases. Mg-free gelatin gel also shows the highest stress values for given horizontal displacements, while the lowest stress values correspond to the gelatin gel with the highest Mg content.

The shear stress-strain curves shown in Fig. 6b illustrate the contrast between the mechanical responses of gelatin and silica gels. While, as explained above, the mechanical response of gelatin hydrogels can be described as elasto-plastic, with a marked continuous hardening under strain, silica hydrogel shear stress-strain curves are characterized by an initial stress increase to reach a maximum, which is followed by a stress decrease and finally a stress plateau at high strain values. It is worthwhile to note that the addition of $MgCl_2$ to the silica gel significantly shifts the position of the maximum stress towards larger values of horizontal displacement, as evidenced by comparing shear stress-strain curves of Mg-free and 0.1 M $MgCl_2$-bearing silica hydrogels (Fig. 6b). Slip failure was not observed in any of the samples in the considered range of horizontal displacements.
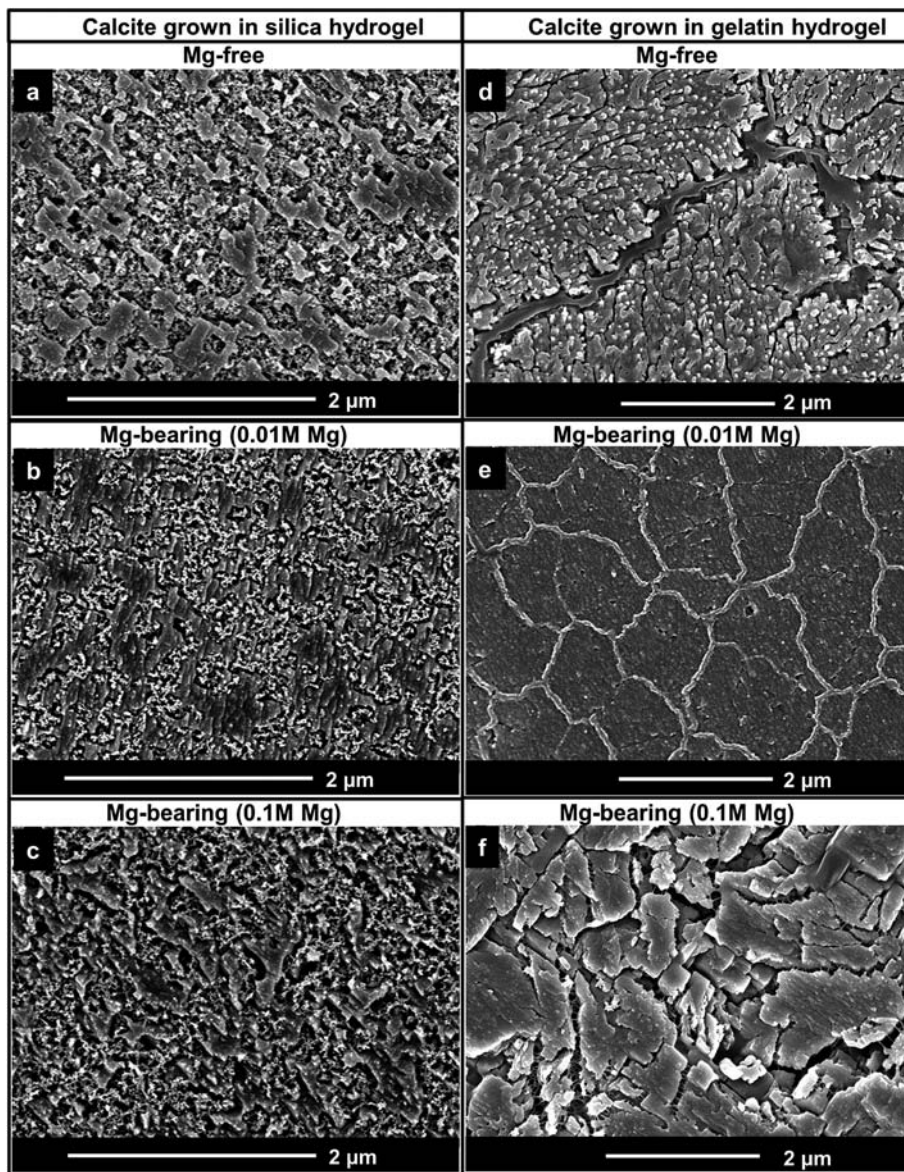
Fig. 3. FE-SEM images of microtome cut, polished, etched and critical point dried surfaces showing gel/calcite composites that were obtained from silica (a–c) and gelatin (d–f) hydrogels without (a, d) and with (b, c, e, f) the presence of Mg in the growth medium. In the case of calcite that grew in silica gel, a decrease in the size of the mineral units in the composite correlates with an increase in Mg in the growth medium. In calcite/gelatin gel aggregates, those formed in Mg-free growth environments show thick membranes separating large mineral subunits (d). Gelatin membranes, though less thick than in aggregates formed in the absence of Mg, are also present in aggregates grown in the presence of low Mg concentrations, where they form sheaths around irregularly sized mineral units (e). No membranes are observed in aggregates formed in gelatin bearing high Mg concentration, where the occluded gel matrix is present as a dense network of fibres that infiltrates calcite with a blocky appearance.

4. Discussion

4.1. Hydrogel incorporation and formation of gel/calcite composites

The incorporation of hydrogel matrices into calcite aggregates was early reported (Nickl & Henisch, 1969) and was subsequently investigated in great detail for a large variety of gels (Grassmann *et al.*, 2002; Li & Estroff, 2007; Huang *et al.*, 2008; Li & Estroff, 2009; Simon *et al.*, 2011; Li *et al.*,

2011a; Asenath-Smith *et al.*, 2012; Nindiyasari *et al.*, 2014a, b, 2015). Ca-Carbonate biominerals in mollusk and brachiopod shells also commonly show occlusion of biologic polymers which are present during their growth (Nindiyasari *et al.*, 2015). The gel-incorporation observed in the present paper leads to mesocrystals which are composites formed as the crystallization of the calcite percolates through the gels. The crystal faces and growth terraces reflect the characteristic geometry of the rhombohedral unit cell of calcite. Thus, these mesocystals form by classical
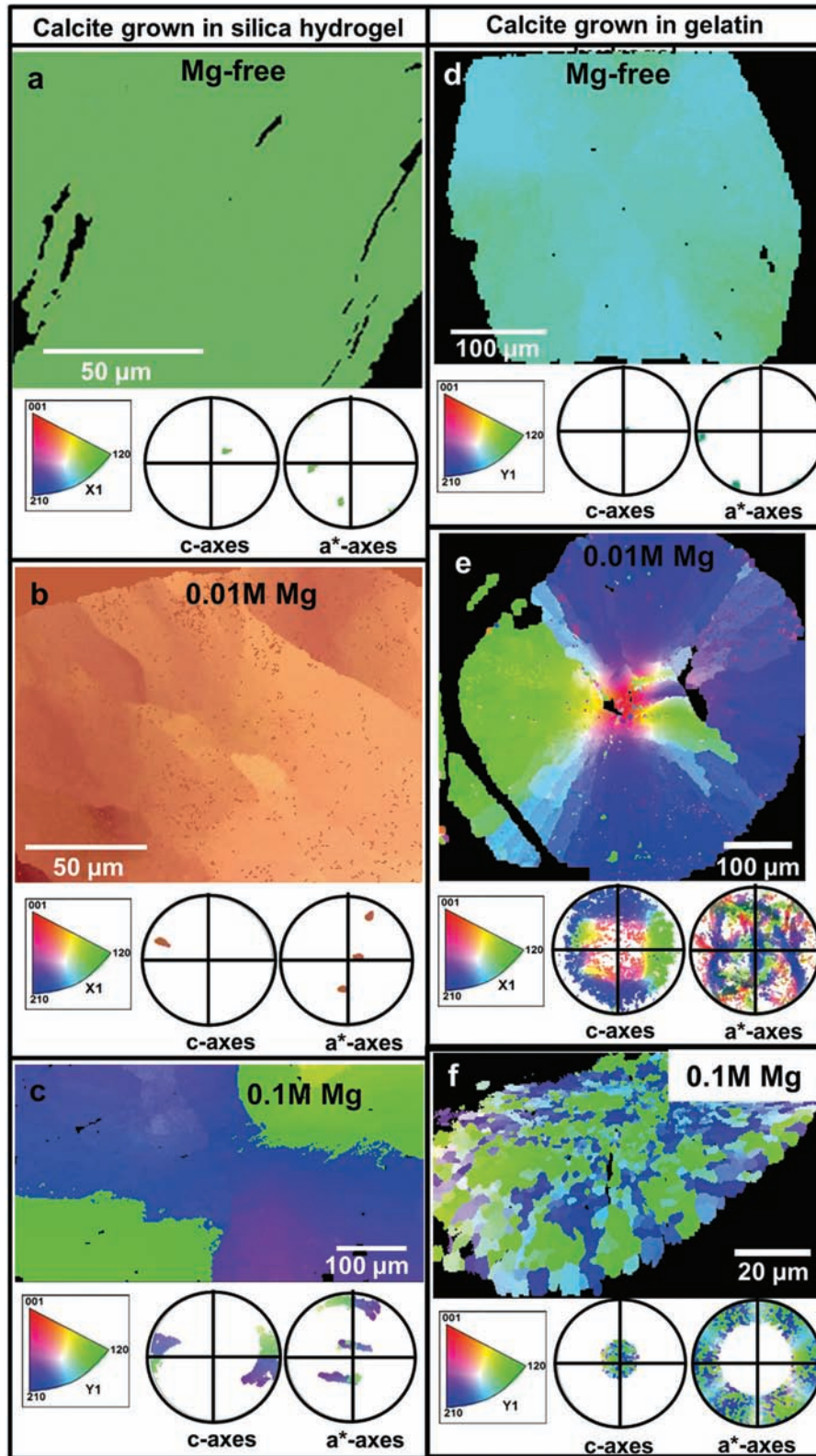
Fig. 4. Calcite orientation results derived from EBSD. Crystal orientation is presented colour-coded in EBSD maps and corresponding pole figures. The used colour code is given at each EBSD map. Figures a–c show orientation patterns for calcite grown in silica gel. Figures d–f show orientation patterns for calcite aggregates obtained in gelatin gel. (a, d) Mg-free growth environment, (b, c, e, f) Mg-containing growth environment. An increase in Mg induces the development of small and large angle boundaries resulting in a mesoscale structuring of the aggregate.
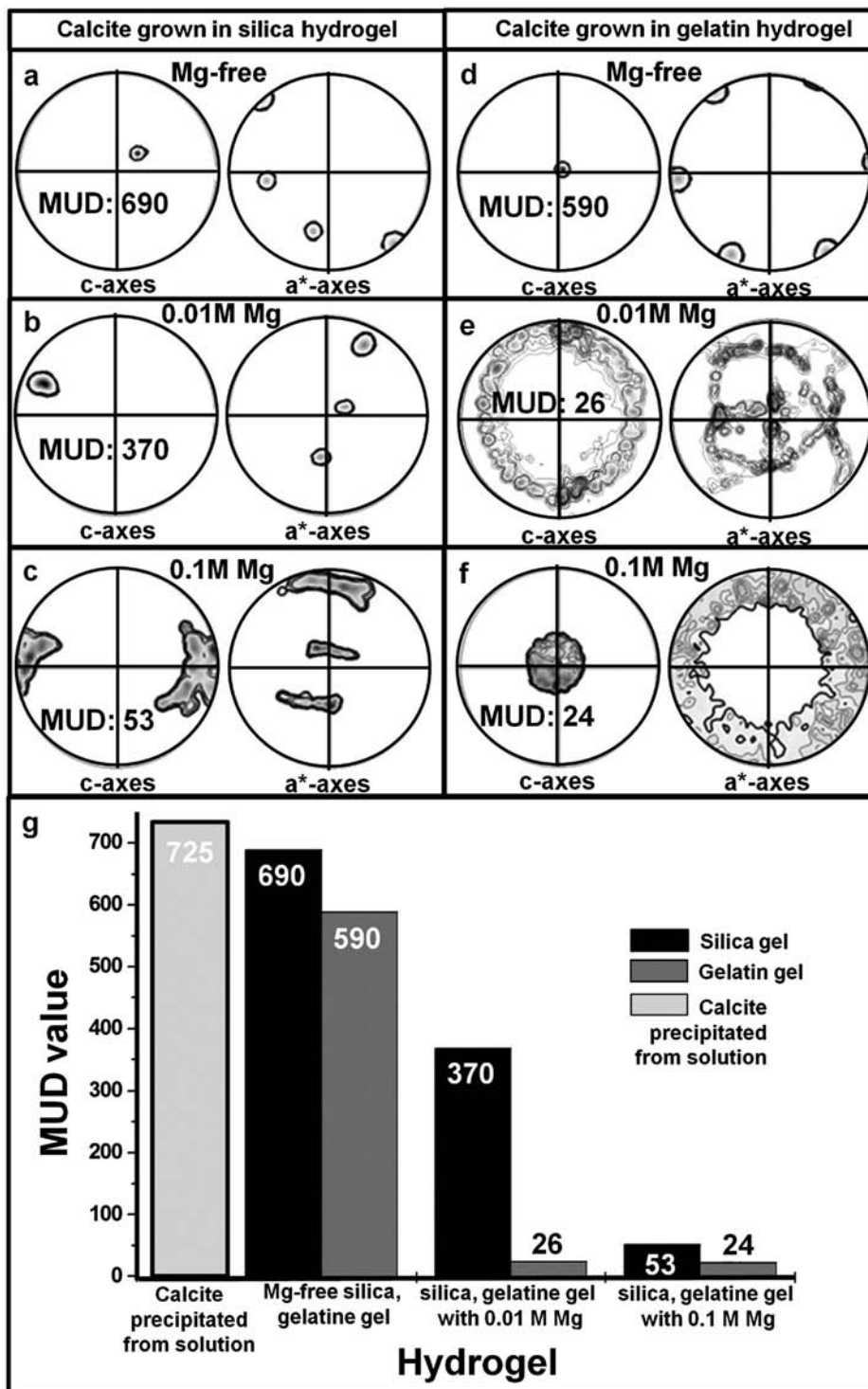
Fig. 5. Texture sharpness in the investigated aggregates. Calcite co-orientation is expressed as multiples of uniform (random) orientation (MUD). Calcite single crystal has a MUD of 725, while all other aggregates show lower MUD values due to the incorporated gel matrix. In Mg-free environments the gel network has little effect on the mesoscale structure of calcite and the aggregate is close to a single crystal, though the effect of gelatin gel occlusion is significantly higher than that of silica gel. The addition of Mg drastically changes the microstructure and texture and initiates the high hierarchical misorientation of calcite within the aggregate.Shear stress as a function of horizontal displacement. (a) Shear stress-strain curves of gelatin gel free of Mg and containing 0.01 M and 0.1 M MgCl$_2$. The three gelatin samples show a distinct elasto-plastic behaviour, characterized by a marked strain hardening with deformation. (b) Comparison of the shear stress-strains curves of Mg-free gelatin gel, Mg-free silica gel and 0.1 M Mg-bearing silica gel. While gelatin gel has an elasto-plastic behaviour under applied shear stress, silica gel shear strength-shear strain curves show a maximum value that shifts towards larger displacements with higher Mg contents. The shape of these curves is compatible with a more brittle behaviour of silica gel. Neither gelatin gel nor silica gel samples show any evidence of slip failure in the range of strain explored.

Fig. 6. Shear stress as a function of horizontal displacement. (a) Shear stress-strain curves of gelatin gel free of Mg and containing 0.01 M and 0.1 M MgCl$_2$. The three gelatin samples show a distinct elasto-plastic behaviour, characterized by a marked strain hardening with deformation. (b) Comparison of the shear stress-strains curves of Mg-free gelatin gel, Mg-free silica gel and 0.1 M Mg-bearing silica gel. While gelatin gel has an elasto-plastic behaviour under applied shear stress, silica gel shear strength-shear strain curves show a maximum value that shifts towards larger displacements with higher Mg contents. The shape of these curves is compatible with a more brittle behaviour of silica gel. Neither gelatin gel nor silica gel samples show any evidence of slip failure in the range of strain explored.

atom-by-atom growth rather than by an assembly of nanoparticles of either calcite or any other transient phase. Accordingly, the observed co-orientation characteristics of the composite mesocrystals simply derive from classical crystal growth, and no complex co-orientation mechanism of hypothetical nanoparticles needs to be hypothesized. Even though hydrogel incorporation into calcite is a general phenomenon, the characteristics of incorporation are variable and depend mainly on the type of the used gel and the concentration of the solid within the gel (Nindiyasari et al., 2014a, 2015). Estroff and co-workers characterized major parameters that control hydrogel incorporation into calcite (Nickl & Henisch, 1969; Li & Estroff, 2007; Kosanovic et al., 2011) and based their approach on the force completion model for crystallization (Chernov et al., 1976; 1977; Chernov & Temkin, 1977; Chernov, 1984), a model developed to describe crystallization in the presence of particles. Following this model Estroff and collaborators defined crystallization pressure and gel strength as the major controlling parameters for the incorporation of the gel into the growing crystal. The crystallization pressure is the pressure that the growing crystal exerts against the growth medium. It increases with the growth rate and, consequently, with the supersaturation (Chernov, 1984; De Yoreo & Vekilov, 2003). The gel strength defines the maximum crystallization pressure that the hydrogel network can resist without breaking or being pushed aside (Asenath-Smith et al., 2012). The balance between crystallization pressure and gel strength defines the amount of hydrogel network that is incorporated into calcite crystals during their growth. Higher growth rates and stronger hydrogels favour higher degrees of gel network incorporation, whereas low growth rates and weak hydrogels result in the gel network being pushed aside during crystallization (Asenath-Smith et al., 2012, Greiner et al., 2018).

4.2. Micro- and nanostructural organization of calcite in silica gel/calcite aggregates

Further advances in understanding the formation of gel/calcite composites result from the detailed characterization of micro and nanostructural features of the aggregates (Nindiyasari et al., 2014a, b, 2015; Greiner et al., 2018). The comparison of composites formed in silica and gelatin gels (see also Nindiyasari et al., 2015) highlights important differences in the ways in which the gel network is occluded into and organized within the growing mineral. These differences entail distinct features of calcite co-orientation patterns. The observed microstructural characteristics of calcite-silica gel composites can be explained with the simple model proposed by Estroff and collaborators (Asenath-Smith et al., 2012) to explain the relationship of growth rate and gel strength with gel occlusion. The addition of Mg to the growth environment, in the case of silica gel, has a further effect related to the incorporation of Mg into calcite structure, in amounts that are always low but increase with Mg concentration in the growth medium. Mg incorporation has a twofold effect on calcite assembly and growth: (i) it increases the solubility of calcite and (ii) it generates lattice strain in the calcite structure. The first effect decreases the crystallization pressure because for given physico-chemical conditions the supersaturation of the system with respect to Mg-bearing calcite is lower than with respect to pure calcite. Moreover, a further decrease in the growth rate will result from the inhibiting effect of Mg on calcite crystallization (Davis et al., 2000; Astilleros et al., 2003, 2010). As a result, the particles constituting the silica gel network will be rather pushed aside than incorporated within the mineral as a higher Mg concentration determines slower growth rates and lower crystallization pressures. The brittle nature of silica hydrogel also contributes to a low gel occlusion (Nindiyasari et al., 2015). The brittle nature of silica

hydrogel compared to gelatin gel is evident by the different characteristics of the shear strength-strain curves of both materials, as depicted in Fig. 6b. The second effect of Mg on calcite growth, the generation of lattice strain associated with Mg substituting Ca in the calcite structure, leads to the formation of dislocations as a means to release this strain. The distribution of dislocations at regular intervals within the aggregate generates low angle boundaries between crystal subunits (Nindiyasari *et al.*, 2014b, 2015), explaining the increased number of crystal subunits that constitute those composites that formed in the presence of higher Mg concentration. The combination of these two effects explains that the occluded silica network appears more dispersed and is distributed between smaller and more numerous crystal subunits in those calcite/silica gel aggregates grown in silica gels with high Mg concentrations compared to aggregates that formed in silica gel with a low Mg concentration or, even, without Mg. Moreover, the generation of small and large angle boundaries that is associated with the formation of dislocations promotes split growth phenomena and explains the evolution from single mesocrystals to radial aggregates and the decrease in calcite co-orientation (lower MUD values).

4.3. Micro- and nanostructural organization of calcite in gelatin gel/calcite aggregates

Calcite/gelatin composites show a more complex internal structure with regards to both, calcite orientation patterns and gel network distribution and organization. The composites that grow in the absence of Mg contain thick gelatin membranes between the subunits and show a high degree of calcite co-orientation. With the addition of $MgCl_2$ to the growth medium we observe a sudden and strong increase in the number of subunits and calcite misorientation in the composite. This is concomitant to a decrease in the thickness of gelatin membranes. The membranes are absent in composites that form in a high $MgCl_2$ concentration environment.

The membranes observed in composites formed in gelatin gel without Mg or with low Mg contents are the consequence of the mechanical response of gelatin gel to crystallization pressure. Whereas silica hydrogel behaves as a brittle medium, gelatin can deform plastically, as demonstrated by the different characteristics of their shear strength-strain curves (Fig. 6b). When the balance between crystallization pressure and gel strength is such that gelatin fibres are pushed aside by the growing crystal, these fibres are pushed against other fibres and become squeezed together. This determines a local increase in the density of fibres and induces the local reorganization of the gel network, which translates into the formation of gel membranes between the subunits. The characteristic strain hardening displayed by gelatin hydrogels (Fig. 6a) can be the consequence of the ability of gelatin fibres to be squeezed together, leading to a gel density increase as well as reorganization of the gel fabric. Explaining the changes observed in the characteristics of gel membranes with the addition

of Mg requires considering both, those effects resulting from the incorporation of Mg into the calcite structure and the changes in the mechanical response of the gel that are associated with the presence of Mg in the growth medium.

As explained in the previous section for calcite/silica gel composites, the incorporation of Mg into calcite induces lattice strain which is released through the formation of dislocations (Nindiyasari *et al.*, 2014b, 2015). The amount of Mg incorporated into calcite is up to ~5 times higher in gelatin than in silica gel. Consequently, Mg-calcite grown in gelatin gel must contain a much higher density of dislocations. This can explain the strong increase in the number of subunits and calcite misorientation observed with the addition of $MgCl_2$ to the gelatin. However, this explanation cannot account for the differences between composites grown in gelatin gel with low and high Mg since calcite incorporates similar amounts of Mg in both cases. Consequently, in both cases there must be similar densities of Mg-related dislocations. As we have also explained in the previous section, Mg also affects calcite growth by reducing the growth rate. According to the model proposed by Estroff and collaborators (Li *et al.*, 2009, 2011a; Asenath-Smith *et al.*, 2012), a decrease in growth rate leads to a decrease in the amount of gel network that becomes occluded within crystal units. Gelatin fibres being pushed aside rather than incorporated into the growing crystal should lead to the formation of thicker gel membranes. This is in contradiction with observations of gel distribution in calcite/gel composites formed in gelatin with low and high $MgCl_2$ contents. The fact that membranes are thinner in composites formed in gelatin with low Mg and are absent in gelatin with high Mg could be explained if the reduction in calcite growth rate were overbalanced by an effect of Mg on the mechanical properties of gelatin gel. Indeed, it has been proposed based on computer simulations that the stiffness of gelatin fibres is significantly affected by the presence of different elements, mostly divalent cations like Mg^{2+}, in the growth medium (Tlatlik *et al.*, 2006). Our results also point in this direction as evidenced by the different shear stress-strain curves of gelatin gels with different Mg Cl_2 contents (Fig. 6a). A less plastic behaviour of gelatin fibres associated with higher amounts of $MgCl_2$ present in the growth medium would translate into the formation of thinner to inexistent membranes, as it is observed in the calcite-gelatin composites. The increase in the number of subunits when crystal growth takes place in the presence of Mg could be then the consequence of an increase in lattice strain associated with Mg incorporation into calcite structure, to which the occlusion of gelatin fibres within the mineral adds up. Indeed, microstrain fluctuations and decreased grain sizes are associated with the presence of an occluded organic phase in biogenic crystals (Pokroy *et al.*, 2006a, b). However, further investigations that provide a better understanding of both, (i) the influence of Mg on the microscopic, as well as macroscopic, mechanical properties of gelatin gel and (ii) the relationship between gelatin fibres occlusion are still required to fully validate our interpretations.

5. Conclusions

In this study we investigated the effect of magnesium on calcite/gel mesostructure and strength of co-orientation for gel/mineral aggregates grown in two distinct gels: silica and gelatin.

Our study addresses two questions: (i) whether the gel or the cation exchange exerts a more profound effect on mesostructural organization and (ii) whether the cation affects physical properties of the hydrogel as well as the characteristics of the mineral component. Our results show, that even though the two investigated gels are distinct, similar developments of crystal organization can be observed. When aggregates crystallize in growth environments devoid of magnesium, we obtain mesocrystals for both gels with overall single-crystal-like co-orientation. When magnesium is added to the growth medium, the characteristics of the fabric of the gel incorporated into calcite change. This change correlates with the formation of calcite/gel composites which consist of a higher number of mutually misoriented subunits. In the case of silica gel, these composites are radial aggregates with some subunits, while in the case of gelatin gel these composites appear as spherulites. The effect of magnesium is more pronounced in those composites that formed in gelatin gel. This marked effect is consistent with the significantly higher incorporation of Mg into the mineral component of composites that formed in gelatin gel, compared to composites that formed in silica gel. Furthermore, our results confirm that the presence of Mg in the growth medium influences the mechanical response of both gels. This influence is a decrease in elasticity as the concentration of Mg is higher in the case of gelatin gel, while silica gel shows more complex characteristics. The very different mechanical response of silica and gelatin gels, as well as the distinct effect that the addition of Mg to the growth medium has in each case, partially explain the observed different patterns of gel matrix distribution within the different types of calcite/gel composites.

References

ASTM D 3080, (2011): Standard test method for direct shear test of soils. ASTM International, West Conshohocken, PA.

Addadi, L., Joester, D., Nudelman, F., Weiner, S. (2006): Mollusk shell formation: A source of new concepts for understanding biomineralization processes. *Chem. Eur. J.*, **12**, 980–987.

Aizenberg, J., Hanson, J., Koetzle, T.F., Leiserowitz, L., Weiner, S., Addadi, L. (1995): Biologically induced reduction in symmetry – A study of crystal texture of calcitic sponge spicules. *Chem. Eur. J.*, **1**, 414–422.

Alvares, K., Dixit, S.N., Lux, E., Veis, A. (2009): Echinoderm phosphorylated matrix proteins UTMP16 and UTMP19 have different functions in sea urchin tooth mineralization. *J. Biol. Chem.*, **284**, 26149–26160.

Asenath-Smith, E., Li, H.Y., Keene, E.C., Seh, Z.W., Estroff, L.A. (2012): Crystal growth of calcium carbonate in hydrogels as a model of biomineralization. *Adv. Funct. Mater.*, **22**, 2891–2914.

Astilleros, J.M., Fernández-Díaz, L., Putnis, A. (2010): The role of magnesium in the growth of calcite: An AFM study. *Chem. Geol.*, **271**, 52–58.

Astilleros, J.M., Pina, C.M., Fernández-Díaz, L., Putnis, A. (2003): Nanoscale growth of solids crystallising from multicomponent aqueous solutions. *Surf. Sci.*, **545**, L767–L773.

Bar-On, B. & Wagner, H.D. (2013): Structural motifs and elastic properties of hierarchical biological tissues – A review. *J. Struct. Biol.* **183**, 149–164.

Bar-On, B. & Wagner, H.D. (2013): Structural motifs and elastic properties of hierarchical biological tissues – A review. *J. Struct. Biol.* **183**, 149–164.

Bentov, S. & Erez, J. (2006): Impact of biomineralization processes on the Mg content of foraminiferal shells: A biological perspective. *Geochem. Geophys. Geosyst.*, **7**, 1–11.

Blank, S., Arnoldi, M., Khoshnavaz, S., Treccani, L., Kuntz, M., Mann, K., Grathwohl, G., Fritz, M. (2003): The nacre protein perlucin nucleates growth of calcium carbonate crystals. *J. Microsc.*, **212**, 280–291.

Cartwright, J.H.E., Checa, A.G., Gale, J.D., Gebauer, D., Sainz-Díaz, C.I. (2012): Calcium carbonate polyamorphism and its role in biomineralization: How many amorphous calcium carbonates are there? *Angew. Chem. Int. Ed.*, **51**, 11960–11970.

Checa, A.G., Cartwright, J.H.E., Willinger, M.G. (2011): Mineral bridges in nacre. *J. Struct. Biol.*, **176**, 330–339.

Cheng, X.G. & Gower, L.B. (2006): Molding mineral within microporous hydrogels by a polymer-induced liquid-precursor (PILP) process. *Biotechnol. Progr.*, **22**, 141–149.

Chernov, A.A. (1984): Modern crystallography III: Crystal growth. Springer-Verlag, Berlin Heidelberg, 517 p.

Chernov, A.A. & Temkin, D.E. (1977): Capture of inclusions in crystal growth. *in* "Crystal growth and materials: Review papers of the first European conference on crystal growth ECCG-1, Zurich", Kaldis, E. & Scheel, H.J., eds. North-Holland Pub. Co., Amsterdam, 4–77.

Chernov, A.A., Temkin, D.E., Mel'nikova, A.M. (1976): Theory of the capture of solid inclusions during the growth of crystals from the melt. *Sov. Phys. Crystallogr.*, **21**, 369–373.

Chernov, A.A., Temkin, D.E., Mel'nikova, A.M. (1977): The influence of the thermal conductivity of a macroparticle on its capture by a crystal growing from a melt. *Sov. Phys. Crystallogr.*, **22**, 656–658.

Cölfen, H. (2010): Biomineralization: A crystal-clear view. *Nat. Mater.*, **9**, 960–961.

Cölfen, H. & Antonietti, M. (2008): Mesocrystals and nonclassical crystallization. John Wiley & Sons, Ltd, Hoboken, NJ.

Davis, K.J., Dove, P.M., De Yoreo, J.J. (2000): The role of Mg^{2+} as an impurity in calcite growth. *Science*, **290**, 1134–1137.

De Yoreo, J.J. & Vekilov, P.G. (2003): Principles of crystal nucleation and growth. *Biomineralization*, **54**, 57–93.

Dey, A., Bomans, P.H.H., Müller, F.A., Will, J., Frederik, P.M., de With, G., Sommerdijk, N.A.J.M. (2010): The role of prenucleation clusters in surface-induced calcium phosphate crystallization. *Nat. Mater.*, **9**, 1010–1014.

Dorvee, J.R., Boskey, A.L., Estroff, L.A. (2012): Rediscovering hydrogel-based double-diffusion systems for studying biomineralization. *Crystengcomm*, **14**, 5681–5700.

Dunlop, J.W.C. & Fratzl, P. (2013): Multilevel architectures in natural materials. *Scripta Mater.*, **68**, 8–12.

Fabritius, H., Walther, P., Ziegler, A. (2005): Architecture of the organic matrix in the sternal CaCO₃ deposits of *Porcellio scaber* (Crustacea, Isopoda). *J. Struct. Biol.*, **150**, 190–199.

Fernández-Díaz, L., Putnis, A., Prieto, M., Putnis, C.V. (1996): The role of magnesium in the crystallization of calcite and aragonite in a porous medium. *J. Sediment. Res.*, **66**, 482–491.

Fratzl, P. & Weinkamer, R. (2007): Nature's hierarchical materials. *Prog. Mater Sci.*, **52**, 1263–1334.

Fritz, M. & Morse, D.E. (1998): The formation of highly organized biogenic polymer/ceramic composite materials: The high-performance microaluminate of molluscan nacre. *Curr. Opin. Colloid Interface Sci.*, **3**, 55–62.

García-Ruiz, J.M. (1991): The uses of crystal growth in gels and other diffusing-reacting systems. *Key Eng. Mater.*, **58**, 87–106.

García-Ruiz, J.M., Navarro, A.R., Kälin, O. (1995): Textural analysis of eggshells. *Mater. Sci. Eng., C: Biomimetic Mater. Sens. Syst.*, **3**, 95–100.

Gebauer, D. & Cölfen, H. (2011): Prenucleation clusters and non-classical nucleation. *Nano Today*, **6**, 564–584.

Goetz, A.J., Griesshaber, E., Abel, R., Fehr, T., Ruthensteiner, B., Schmahl, W.W. (2014): Tailored order: The mesocrystalline nature of sea urchin teeth. *Acta Biomater.*, **10**, 3885–3898.

Goetz, A.J., Steinmetz, D.R., Griesshaber, E., Zaefferer, S., Raabe, D., Kelm, K., Irsen, S., Sehrbrock, A., Schmahl, W.W. (2011): Interdigitating biocalcite dendrites form a 3-D jigsaw structure in brachiopod shells. *Acta Biomater.*, **7**, 2237–2243.

Gower, L.B. (2008): Biomimetic model systems for investigating the amorphous precursor pathway and its role in biomineralization. *Chem. Rev.*, **108**, 4551–4627.

Grassmann, O., Müller, G., Löbmann, P. (2002): Organic-inorganic hybrid structure of calcite crystalline assemblies grown in a gelatin hydrogel matrix: Relevance to biomineralization. *Chem. Mater.*, **14**, 4530–4535.

Greiner, M., Yin, X., Fernández-Díaz, L., Griesshaber, E., Weitzel, F., Ziegler, A., Veintemillas-Verdaguer, S., Schmahl, W.W. (2018): Combined influence of reagent concentrations and agar hydrogel strength on the formation of biomimetic hydrogel–calcite composites. *Cryst. Growth Des.*, **18**, 1401–1414.

Gries, K., Heinemann, F., Gummich, M., Ziegler, A., Rosenauer, A., Fritz, M. (2011): Influence of the insoluble and soluble matrix of abalone nacre on the growth of calcium carbonate crystals. *Cryst. Growth Des.*, **11**, 729–734.

Griesshaber, E., Schmahl, W.W., Neuser, R., Pettke, T., Blum, M., Mutterlose, J., Brand, U. (2007): Crystallographic texture and microstructure of terebratulide brachiopod shell calcite: An optimized materials design with hierarchical architecture. *Am. Mineral.*, **92**, 722–734.

Griesshaber, E., Schmahl, W.W., Ubhi, H.S., Huber, J., Nindiyasari, F., Maier, B., Ziegler, A. (2013): Homoepitaxial meso- and microscale crystal co-orientation and organic matrix network structure in *Mytilus edulis* nacre and calcite. *Acta Biomater.*, **9**, 9492–9502.

Han, Y.J., Wysocki, L.M., Thanawala, M.S., Siegrist, T., Aizenberg, J. (2005): Template-dependent morphogenesis of oriented calcite crystals in the presence of magnesium ions. *Angew. Chem. Int. Ed.*, **44**, 2386–2390.

Helbig, U. (2008): Growth of calcium carbonate in polyacrylamide hydrogel: Investigation of the influence of polymer content. *J. Cryst. Growth*, **310**, 2863–2870.

Henisch, H.K. (1988): Crystals in gels and liesegang rings. Cambridge University Press, New York, NY.

Huang, Y.X., Buder, J., Cardoso-Gil, R., Prots, Y., Carrillo-Cabrera, W., Simon, P., Kniep, R. (2008): Shape development and structure of a complex (otoconia-like?) calcite-gelatine composite. *Angew. Chem. Int. Ed.*, **47**, 8280–8284.

Huber, J., Fabritius, H.O., Griesshaber, E., Ziegler, A. (2014): Function-related adaptations of ultrastructure, mineral phase distribution and mechanical properties in the incisive cuticle of mandibles of *Porcellio scaber* Latreille, 1804. *J. Struct. Biol.*, **188**, 1–15.

Kim, Y.Y., Schenk, A.S., Ihli, J., Kulak, A.N., Hetherington, N.B.J., Tang, C.C., Schmahl, W.W., Griesshaber, E., Hyett, G., Meldrum, F.C. (2014): A critical analysis of calcium carbonate mesocrystals. *Nat. Commun.*, **5**, 1–14.

Kniep, R. & Simon, P. (2007): Fluorapatite-gelatine-nanocomposites: Self-organized morphogenesis, real structure and relations to natural hard materials. *in* "Biomineralization I: Crystallization and self-organization process", Naka, K., ed., Springer-Verlag Berlin, Berlin, 73–125.

Kocks, U.F., Tomé, C.N., Wenk, H.-R. (2000): Texture and anisotropy-preferred orientations in polycrystals and their effect on materials properties. Cambridge University Press, Cambridge, 692 p.

Kosanovic, C., Falini, G., Kralj, D. (2011): Mineralization of calcium carbonates in gelling media. *Cryst. Growth Des.*, **11**, 269–277.

Li, H.Y. & Estroff, L.A. (2007): Porous calcite single crystals grown from a hydrogel medium. *Crystengcomm*, **9**, 1153–1155.

Li, H.Y. & Estroff, L.A. (2009): Calcite growth in hydrogels: Assessing the mechanism of polymer-network incorporation into single crystals. *Adv. Mater.*, **21**, 470–473.

Li, H.Y., Fujiki, Y., Sada, K., Estroff, L.A. (2011a): Gel incorporation inside of organic single crystals grown in agarose hydrogels. *Crystengcomm*, **13**, 1060–1062.

Li, H.Y., Xin, H.L., Kunitake, M.E., Keene, E.C., Muller, D.A., Estroff, L.A. (2011b): Calcite prisms from mollusk shells (*Atrina rigida*): Swiss-cheese-like organic-inorganic single-crystal composites. *Adv. Funct. Mater.*, **21**, 2028–2034.

Li, H.Y., Xin, H.L., Muller, D.A., Estroff, L.A. (2009): Visualizing the 3D internal structure of calcite single crystals grown in agarose hydrogels. *Science*, **326**, 1244–1247.

Lowenstam, H.A. & Weiner, S. (1989): On Biomineralization. Oxford University Press, New York, NY, 336 p.

Mann, S. (2001): Biomineralization: Principles and concepts in bioinorganic materials chemistry. Oxford University Press, New York, 210 p.

Marin, F. & Luquet, G. (2004): Molluscan shell proteins. *C.R. Palevol*, **3**, 469–492.

Marin, F., Luquet, G., Marie, B., Medakovic, D. (2008): Molluscan shell proteins: Primary structure, origin, and evolution. *Curr. Top. Dev. Biol.*, **80**, 209–276.

Meldrum, F.C. & Cölfen, H. (2008): Controlling mineral morphologies and structures in biological and synthetic systems. *Chem. Rev.*, **108**, 4332–4432.

Nickl, H.J. & Henisch, H.K. (1969): Growth of calcite crystals in gels. *J. Electrochem. Soc.*, **116**, 1258–1260.

Nindiyasari, F., Fernández-Díaz, L., Griesshaber, E., Astilleros, J. M., Sanchez-Pastor, N., Schmahl, W.W. (2014a): Influence of gelatin hydrogel porosity on the crystallization of CaCO₃. *Cryst. Growth Des.*, **14**, 1531–1542.

Nindiyasari, F., Griesshaber, E., Fernández-Díaz, L., Astilleros, J. M., Sanchez-Pastor, N., Ziegler, A., Schmahl, W.W. (2014b): Effects of Mg and hydrogel solid content on the crystallization of calcium carbonate in biomimetic counter-diffusion systems. *Cryst. Growth Des.*, **14**, 4790–4802.

Nindiyasari, F., Ziegler, A., Griesshaber, E., Fernández-Díaz, L., Huber, J., Walther, P., Schmahl, W.W. (2015): Effect of hydrogel matrices on calcite crystal growth morphology, aggregate formation, and co-orientation in biomimetic experiments and biomineralization environments. *Cryst. Growth Des.*, **15**, 2667–2685.

Nudelman, F., Gotliv, B.A., Addadi, L., Weiner, S. (2006): Mollusk shell formation: Mapping the distribution of organic matrix components underlying a single aragonitic tablet in nacre. *J. Struct. Biol.*, **153**, 176–187.

Otalora, F., Gavira, J.A., Ng, J.D., García-Ruiz, J.M. (2009): Counterdiffusion methods applied to protein crystallization. *Prog. Biophys. Mol. Biol.*, **101**, 26–37.

Pokroy, B. & Aizenberg, J. (2007): Calcite shape modulation through the lattice mismatch between the self-assembled monolayer template and the nucleated crystal face. *Crystengcomm*, **9**, 1219–1225.

Pokroy, B., Fitch, A.N., Lee, P.L., Quintana, J.P., Caspi, E.N., Zolotoyabko, E. (2006): Anisotropic lattice distortions in the mollusk-made aragonite: A widespread phenomenon. *J. Struct. Biol.*, **153**, 145–150.

Pokroy, B., Fitch, A.N., Marin, F., Kapon, M., Adir, N., Zolotoyabko, E. (2006): Anisotropic lattice distortions in biogenic calcite induced by intra-crystalline organic molecules. *J. Struct. Biol.*, **155**, 96–103.

Politi, Y., Levi-Kalisman, Y., Raz, S., Wilt, F., Addadi, L., Weiner, S., Sagi, I. (2006): Structural characterization of the transient amorphous calcium carbonate precursor phase in sea urchin embryos. *Adv. Funct. Mater.*, **16**, 1289–1298.

Robach, J.S., Stock, S.R., Veis, A. (2005): Transmission electron microscopy characterization of macromolecular domain cavities and microstructure of single-crystal calcite tooth plates of the sea urchin *Lytechinus variegatus*. *J. Struct. Biol.*, **151**, 18–29.

Robach, J.S., Stock, S.R., Veis, A. (2009): Structure of first- and second-stage mineralized elements in teeth of the sea urchin *Lytechinus variegatus*. *J. Struct. Biol.*, **168**, 452–466.

Sancho-Tomás, M., Fermani, S., Durán-Olivencia, M.A., Otálora, F., Gómez-Morales, J., Falini, G., García-Ruiz, J.M. (2013): Influence of charged polypeptides on nucleation and growth of $CaCO_3$ evaluated by counterdiffusion experiments. *Cryst. Growth Des.*, **13**, 3884–3891.

Sancho-Tomás, M., Fermani, S., Gómez-Morales, J., Falini, G. & García-Ruiz, J.M. (2014a): Calcium carbonate bio-precipitation in counter-diffusion systems using the soluble organic matrix from nacre and sea-urchin spine. *Eur. J. Mineral.* **26**, 523–535.

Sancho-Tomás, M., Fermani, S., Goffredo, S., Dubinsky, Z., Garcia-Ruiz, J.M., Gomez-Morales, J., Falini, G. (2014b): Exploring coral biomineralization in gelling environments by means of a counter diffusion system. *Crystengcomm*, **16**, 1257–1266.

Seidl, B., Huemer, K., Neues, F., Hild, S., Epple, M., Ziegler, A. (2011): Ultrastructure and mineral distribution in the tergite cuticle of the beach isopod *Tylos europaeus* Arcangeli, 1938. *J. Struct. Biol.*, **174**, 512–526.

Sethmann, I., Helbig, U., Worheide, G. (2007): Octocoral sclerite ultrastructures and experimental approach to underlying biomineralisation principles. *Crystengcomm*, **9**, 1262–1268.

Sethmann, I. & Worheide, G. (2008): Structure and composition of calcareous sponge spicules: A review and comparison to structurally related biominerals. *Micron*, **39**, 209–228.

Simon, P., Carrillo-Cabrera, W., Formánek, P., Göbel, C., Geiger, D., Ramlau, R., Tlatlik, H., Buder, J., Kniep, R. (2004): On the real-structure of biomimetically grown hexagonal prismatic seeds of fluorapatite-gelatine-composites: TEM investigations along [001]. *J. Mater. Chem.*, **14**, 2218–2224.

Simon, P., Carrillo-Cabrera, W., Huang, Y.X., Buder, J., Borrmann, H., Cardoso-Gil, R., Rosseeva, E., Yarin, Y., Zahnert, T., Kniep, R. (2011): Structural relationship between calcite-gelatine composites and biogenic (human) otoconia. *Eur. J. Inorg. Chem.*, 5370–5377.

Sugawara, A., Ishii, T., Kato, T. (2003): Self-organized calcium carbonate with regular surface-relief structures. *Angew. Chem. Int. Ed.*, **42**, 5299–5303.

Sunaband, J. & Bhushan, B. (2012): Hierarchical structure and mechanical properties of nacre: a review. *RSC Adv.* **2**, 7617–7632.

Tlatlik, H., Simon, P., Kawska, A., Zahn, D., Kniep, R. (2006): Biomimetic fluorapatite-gelatine nanocomposites: Pre-structuring of gelatine matrices by ion impregnation and its effect on form development. *Angew. Chem. Int. Ed.*, **45**, 1905–1910.

Wang, T.X., Xu, A.W., Cölfen, H. (2006): Formation of self-organized dynamic structure patterns of barium carbonate crystals in polymer-controlled crystallization. *Angew. Chem. Int. Ed.*, **45**, 4451–4455.

Weiner, S. & Addadi, L. (2011): Crystallization pathways in biomineralization. *in* "Annual review of materials research, vol 41", Clarke, D.R. & Fratzl, P., eds. Annual Reviews, Palo Alto, 21–40.

Weiner, S. & Traub, W. (1980): X-ray diffraction study of the insoluble organic matrix of mollusk shells. *FEBS Lett.*, **111**, 311–316.

Wolf, S.E., Muller, L., Barrea, R., Kampf, C.J., Leiterer, J., Panne, U., Hoffmann, T., Emmerling, F., Tremel, W. (2011): Carbonate-coordinated metal complexes precede the formation of liquid amorphous mineral emulsions of divalent metal carbonates. *Nanoscale*, **3**, 1158–1165.